A high-frequency flexible symmetric supercapacitor prepared by the laser-defocused ablation of MnO_2 on a carbon cloth

ZHAO Guang-yao[1], WANG Fang-cheng[1], LIU Ming-jie[1], SUI Yi-ming[2], ZHANG Zhuo[1], KANG Fei-yu[1], YANG Cheng[1,*]

(1. *Institute of Materials Research*, *Tsinghua Shenzhen International Graduate School*, *Tsinghua University*, *Shenzhen* 518055, *China*; 2. *Department of Chemistry*, *Oregon State University*, *Corvallis*, 97331-4003, *USA*)

Abstract: The rapid development of flexible electronics has produced an enormous demand for supercapacitors. Compared to batteries, supercapacitors have great advantages in terms of power density and cycling stability. They can also respond well on a time scale of seconds, but most have a poor frequency response, and behave more like pure resistors when used at high frequencies (e.g., above 100 Hz). It is therefore challenging to develop supercapacitors that work at a frequency of over 100 Hz. We report a high-frequency flexible symmetrical supercapacitor composed of a MnO_2@carbon cloth hybrid electrode (CC@MnO_2), which is synthesized by the defocused-laser ablation method. This CC@MnO_2-based symmetric supercapacitor has an excellent specific areal capacitance of 1.53 mF cm^{-2} at a frequency of 120 Hz and has good cycling stability with over 92.10% capacitance retention after 100 000 cycles at 100 V s^{-1}. This remarkable electrochemical performance is attributed to the combined effect of the high conductivity of the 3D structure of the carbon cloth and the exceptional pseudo-capacitance of the laser-produced MnO_2 nanosheets. The defocused laser ablation method can be used for large-scale production using roll-to-roll technology, which is promising for the wide use of the supercapacitor in high-frequency electronic devices.

Key words: High-frequency supercapacitors; Defocused-laser ablation method; Flexible electrode; Manganese dioxide (MnO_2); Carbon cloth

1 Introduction

Rapid increasing demands of the portable miniaturized electronics have encouraged the development of the energy storing devices, particularly the supercapacitors, which is attractive due to the advantages of fast charging/discharging rate, high power density, and long cycling life compared with batteries. Nevertheless, the supercapacitors perform weakly as filtering capacitors due to the serious drop of supercapacitors' capacitance using alternating current (AC). Most supercapacitors always have poor frequency response when used at a high frequency (e.g., above 100 Hertz), and behave more like pure resistors[1]. Therefore, the high-frequency supercapacitors (HFSCs) which mean they can work surpass 100 Hz with almost no thermosteresis have been a challenging task.

So far various researches have been carried out to realize the HFSCs. Miller *et al.* firstly fabricated vertically oriented graphene sheets with open pores on the nickel for a high-frequency supercapacitor, which delivered a specific areal capacitance (CA) of 0.2 mF cm^{-2} and retained 0.09 mF cm^{-2} at 120 Hz. To date, serval carbon composite materials and polymers such as carbon cloth (CC), reduced graphene oxide (rGO), and conducting polymers have been proposed for HFSCs because the high phase angles are high in the frequency range from tens to hundreds Hz, such as graphene-based HFSCs (80 μF cm^{-2} at 120 Hz), carbon nanotubes-based HFSCs (601 μF cm^{-2} at 120 Hz), and melamine-based HFSCs (132 μF cm^{-2} at 120 Hz). Among them, the poor capacitances seriously limit their performance[2]. The area capacitances of these works are still not comparable with that of the commercial tantalum capacitors (1.5 mF cm^{-2}, Samsung B3528)[1]. To solve this problem, one efficient way is to *in situ* grow pseudocapacitive materials on the CC.

Received date: 2021-09-10; **Revised date:** 2021-11-10

Corresponding author: YANG Cheng. E-mail: yang.cheng@sz.tsinghua.edu.cn

Author introduction: ZHAO Guang-yao. E-mail: zgy19@mails.tsinghua.edu.cn

Pseudocapacitive materials with high specific capacitances are emerging as a promising alternative/complement for the conventional double-layer-type materials. Among them, transition metal oxides (TMOs) are receiving the most interest owing to their particularly high theoretical specific capacitances, such as RuO_3, Co_3O_4, and MnO_2. Besides the high capacitance, MnO_2 outstands in the materials because of its low-cost and environment-benign properties. However, poor electrical conductivity and high charge-transfer resistance of MnO_2 seriously limit the specific capacitance and power characteristics[3].

In present study, MnO_2 nanosheets were grown on the CC by the defocused-laser ablation method. Compared with other ways (*e.g.,* electro-deposition[3] and hydrothermal[4]), the defocused-laser ablation method could not only reduce $Mn(AC)_2$ to MnO_2 on the CC, but had a great advantage in pattern and mass production. Besides, as-prepared LCC@MnO_2 symmetric supercapacitor exhibited the high CA of 1.53 mF cm^{-2} at 120 Hz and excellent cycle stability (the capacity maintained over 92.10% after 100 000 cycles at 100 V s^{-1}). Also, the method presents potentials on preparing flexible electrodes. The device based on the LCC@MnO_2 electrode showed a stable capacitance performance when bent in different angles (0°-180°) and good cycle stability (104.40% capacitance retention after 10 000 cycles at 100 V s^{-1}).

2 Experimental

2.1 Materials

All chemicals were analytical reagents and used directly. The carbon cloth (CC, wos 1009) was obtained from Taiwan Tanneng company (thickness: 0.41 mm, China). Manganous acetate ($Mn(AC)_2$) was obtained from Aladdin. Sodium sulphate ($Na_2(SO)_4$) was obtained from Alfa Aesar. Deionized (DI) water was obtained from a Milli-Q system (Millipore).

2.2 Growth of MnO_2 on CC

Inspired by the previous work, defocused laser induced graphene[5] helps to make the energy distribution uniformly. By changing the distance of z-axis to the focal plane, different spot sizes and energy distribution can be acquired. Using a suitable spot size, the processing speed will be increased and the risk of sample burning due to high temperature is also reduced[6]. This work involved this method to treat CC to make MnO_2 nanosheets generate on the surface. The carbon cloth was cut into pieces of CC (1×1 cm^2) and then treated by infrared laser first to improve surface morphology to enhance wettability. 100 μL of 0.5 mol L^{-1} $Mn(Ac)_2$ solution was dipped and coated on the CC and then the LCC/$Mn(AC)_2$ was dried in air for 3 h. After that, the dried materials were ablated through laser processing at a power of 4.2 W, a speed of 50 mm s^{-1}, a step size of 1 064 nm, a diameter of spot of 141.47 μm, and a defocus distance of 10 mm to form LCC@MnO_2 composites. Then, the electrode was dried at 60 °C overnight. The illustration of the preparation of the LCC@MnO_2 electrode is shown in Scheme 1.

2.3 Structure characterization

Field emission scanning electron microscopy (HITACHI SU8010) was used to analyze the morphologies of LCC@MnO_2. X-ray diffraction (Bruker D8

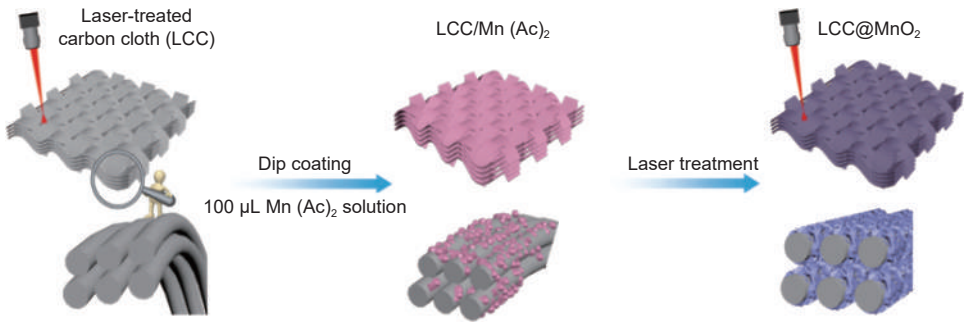

Scheme 1　Schematic representation of the preparation of the MnO_2@LCC electrode.

Advance) by Cu $K\alpha$ radiation with λ=0.154 18 nm (The diffraction angle was from 10° to 85°, and the scanning rate was 5° min^{-1}) was applied to characterize the crystallographic information of LCC and LCC@MnO_2. Laser Microscopic confocal Raman spectroscopy (Horiba LabRAM HR800) was used to obtain the Raman spectra, The transmission electron microscopy (TEM) images were recorded by the FEI Tecnai G2 spirit and the LCC@MnO_2 was cut into some pieces and then dispersed to the supporting carbon films. The X-ray photoelectron spectroscopy (XPS) of the materials was tested by a PHI5000VersaProbeII.

All electrochemical measurements were carried out on the electrochemical station (CHInstruments, Inc., Shanghai). Cyclic voltammetry (CV), galvanostatic charging/discharging (GCD) were tested and electrochemical impedance spectra (EIS) of the studied electrodes were carried out from 100 kHz to 0.01 Hz. The LCC@MnO_2 electrode was examined by a traditional three-electrode system. The symmetric supercapacitor was measured by a coin cell system. The electrolyte was 1 mol L^{-1} Na_2SO_4 solution. During CV and GCD tests, the potential window of the LCC@MnO_2 electrode was from 0 to 0.8 V, the potential window of the symmetric device was from 0 to 1.6 V.

The CA values were obtained from the data of the CV curves using the following equation[1]:

$$C_A = \frac{1}{2 \times A \times v \times \Delta V} \int I(V)\,dV$$

Where A is the area of the working electrode (cm^2), v is the voltage sweep rate (V s^{-1}), ΔV is the applied potential window, and $\int I(V)dV$ is the integral area of the CV curve.

The specific areal capacitance (C_A, μF/cm^2) at different frequencies was calculated by[1]:

$$C_A = -\frac{1}{2\pi f Z'' S}$$

Where f (Hz) is frequency, Z'' (Ω) is the imaginary impedance, and S is the area of electrode.

3 Results and discussion

SEM is applied to investigate the morphologies of the LCC@MnO_2 electrodes (Fig. 1). In Fig. 1a and b, the surface of CC becomes rough after laser treatment and the diameter of the carbon fibers is about 20 μm. According to Fig. 1c and d, the MnO_2 nanosheets can be clearly seen on the carbon fibers. The energy-dispersive spectroscopy (EDS) mapping images indicate the uniform distribution of C, Mn and O elements in the LCC@MnO_2 composites (Fig. 1e). HRTEM image of LCC@MnO_2 illustrates that MnO_2 is successfully anchored to CC through the defocus-laser method. The lattice fringe is 0.45 nm, which is ascribed to the (101) plane about the MnO_2[7]. All of

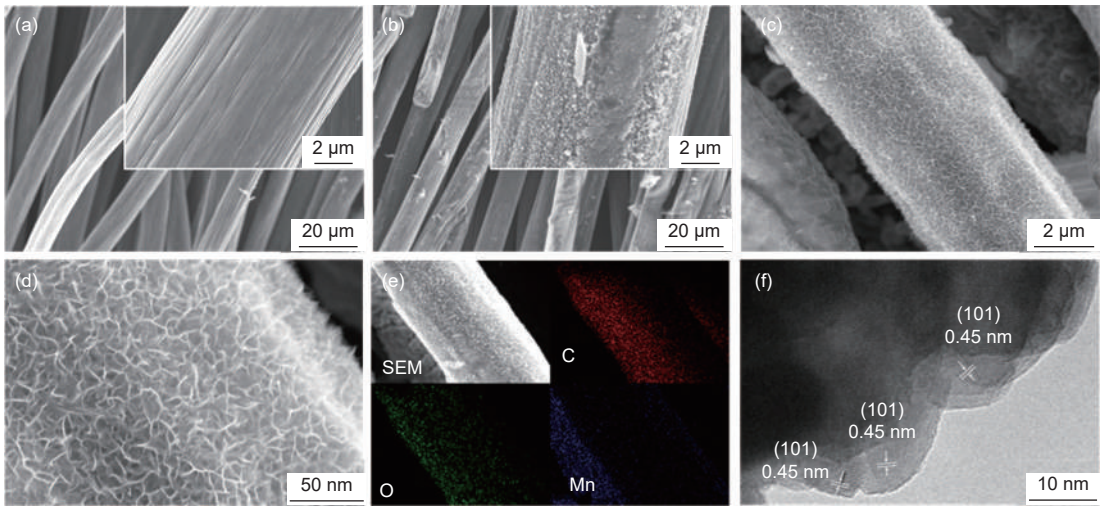

Fig. 1 SEM images of CC (a) before and (b) after laser treatment, (c, d) SEM images of LCC@MnO_2, (e) EDS spectrum of LCC@MnO_2, (f) HRTEM image of LCC@MnO_2.

this prove that the MnO_2 nanosheets are successfully grown on the CC.

The XRD patterns of CC and LCC@MnO_2 samples can be seen in Fig. 2a, the typical C peak can be seen at 2θ = 25.5°, which proves the existence of amorphous graphite carbon of the CC. The diffraction peaks of XRD pattern of LCC@MnO_2 demonstrate the presence of cubic phase α-MnO_2 (JCPDS no. 42-1169) and orthorhombic phase β-MnO_2 (JCPDS no. 50-0866)[7–8]. The Raman spectra of CC and LCC@MnO_2 are shown in Fig. 2b. The two peaks of 1 350 and 1 600 cm^{-1} represent the *D* and *G* peaks of carbon, respectively. The photoinduced defect density is presented by I_D/I_G ratio. The value of I_D/I_G for CC and MnO_2@LCC is 1.05 and 1.17, respectively, which may be due to more defects formed after laser ablation. In addition, the peak of MnO_2 at 646 cm^{-1} can be observed, confirming the successful preparation of MnO_2[7].

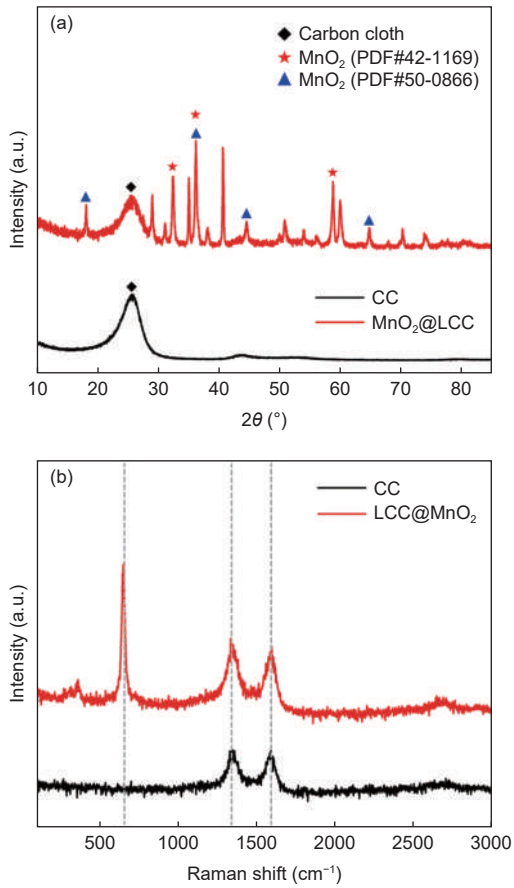

Fig. 2　(a) XRD patterns for CC and LCC@MnO_2. (b) Raman spectra of CC and LCC@MnO_2.

Additionally, as shown in the XPS spectra in Fig. 3a, MnO_2@LCC contains C, O and Mn elements compared to CC. The spectrum of C 1s (Fig. 3b) is fitted into two peaks at 284.8 eV and 286.1 eV, which are assigned to C—C and C=C bonds, respectively. The spectrum of O 1s can be fitted into three peaks with Mn—O—Mn (529.9 eV), Mn—O—H (531.2 eV), and H—O—H (532.6 eV) bonds, as shown in Fig. 3c. From Fig. 3d, two peaks of 641.9 eV and 653.4 eV of Mn 2p spectrum are related to Mn $2p_{3/2}$ and Mn $2p_{1/2}$ of MnO_2, respectively. The spin energy separation between the Mn $2p_{3/2}$ and Mn $2p_{1/2}$ is 11.5 eV, conforming to the reported studies about MnO_2[7].

The performance of LCC@MnO_2 composite is evaluated in 1 mol L^{-1} Na_2SO_4 solution using a traditional three-electrode system. The CV curves of CC, LCC, and LCC@MnO_2 electrodes at 50 mV s^{-1} suggest that CC and LCC contribute negligible capacitance in the LCC@MnO_2 composite electrode (Fig. 4a). As shown in Fig. 4b, although MnO_2 prepared on the carbon fibers increases the resistance, the resistances of these electrodes are still less than 5 Ω, indicating the excellent conductivity of LCC@MnO_2 composite. Fig. 4c and 4d show the CV curves and specific areal capacitance with various scanning rates. The CV curves display a rectangular shape even the scan rate increases to 300 mV s^{-1}, showing excellent capacitive behavior. The CA value is 424 mF cm^{-2} at 2 mV s^{-1}. The GCD curves of LCC@MnO_2 electrode at different current densities are shown in Fig. 4e. They keep a nice linear shape, and the charging/discharging process keeps an excellent symmetry. A high CA value of 672.5 mF cm^{-2} is achieved at 1 mA cm^{-2} for LCC@MnO_2 composite. The capacitance of LCC@MnO_2 composite maintains 106.4% of the origin value after 8 000 cycles (Fig. 4f) as revealed by a cycling test at 100 mV s^{-1}.

The electrochemical performance of a LCC@MnO_2 symmetric supercapacitor is evaluated in a coin cell using 1 mol L^{-1} Na_2SO_4 solution as the electrolyte. Fig. 5a and 5b demonstrate the CV pro-

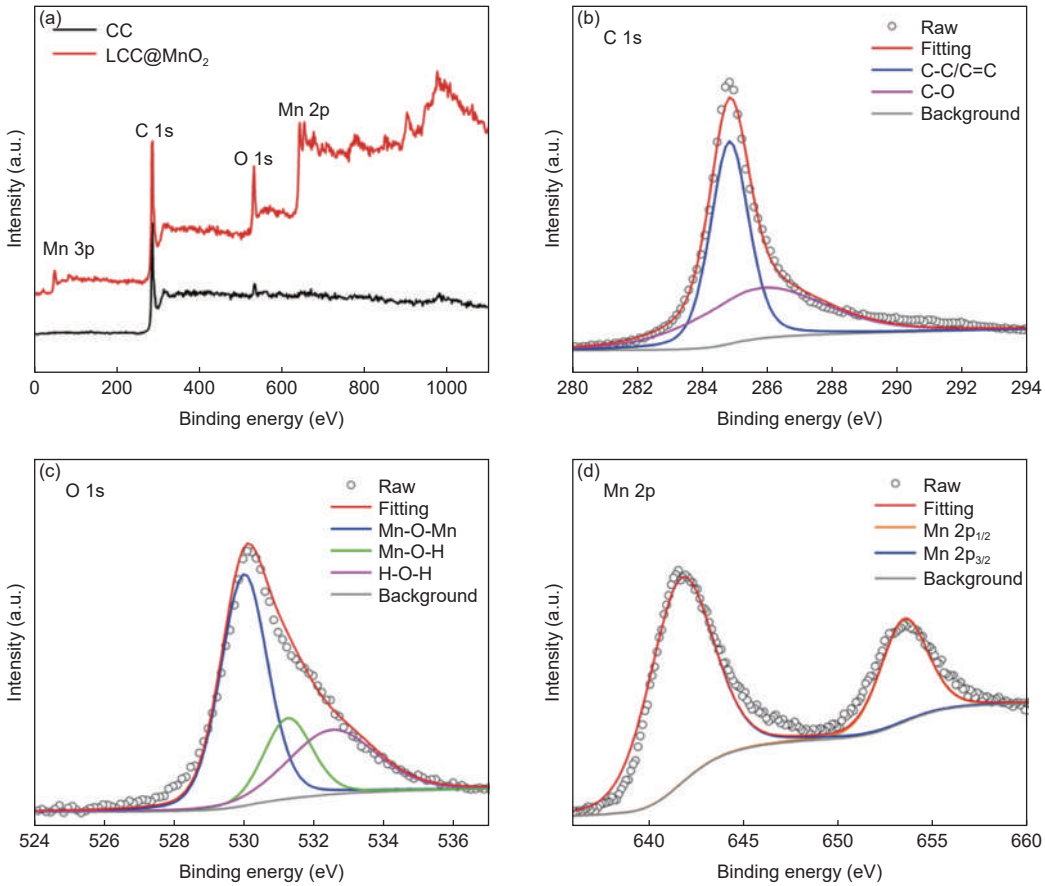

Fig. 3 (a) XPS spectra of the LCC@MnO_2 and CC. High-resolution spectra for (b) C 1s, (c) O 1s and (d) Mn 2p spectra.

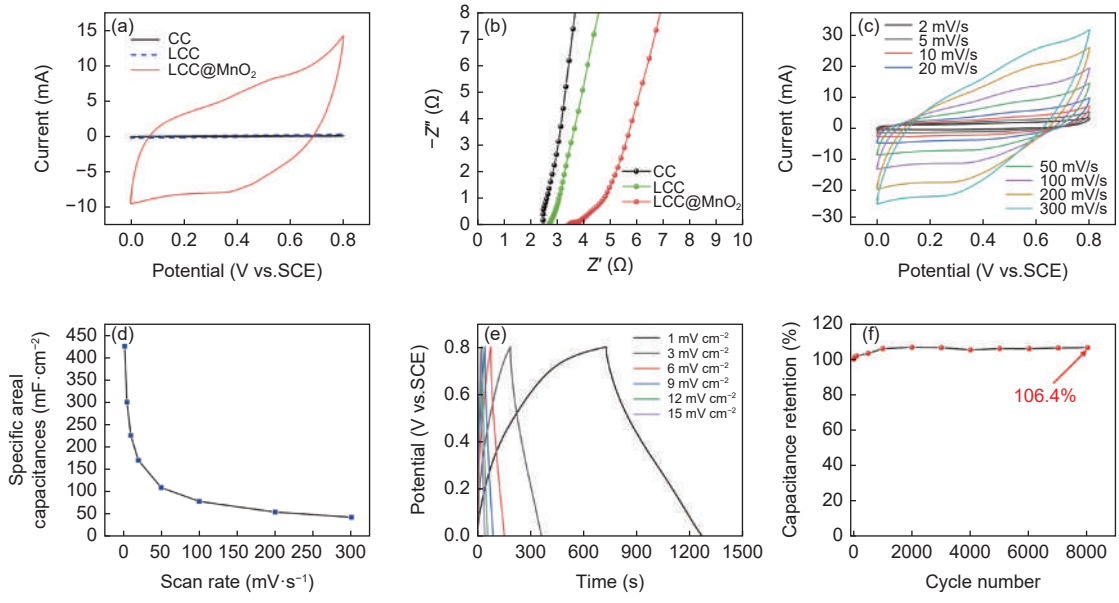

Fig. 4 (a) CV curves of CC, LCC and LCC@MnO_2 at 50 mV/s. (b) EIS characterization for the LCC@MnO_2 electrode. (c) CV curves of LCC@MnO_2 at different scan rates 2-300 mV s^{-1}. (d) The specific areal capacitances of the LCC@MnO_2 electrode at different scan rates. (e) GCD characterization of the LCC@MnO_2 electrode from 1 to 15 mA cm^{-2}. (f) Cycling stability of the LCC@MnO_2 electrode at 100 mV s^{-1}.

files and specific areal capacitance with various scanning rates, respectively. The CV curves present a rectangular shape even the scan rate is increased up to 100 V s^{-1}, showing distinguished high-frequency

capacitive behavior. The CA is 1.5 mF cm^{-2} at 100 V s^{-1}. From Fig. 5c, the LCC@MnO_2 symmetric supercapacitor shows the best specific areal capacitance among the three symmetric supercapacitors at 100 V s^{-1}. Fig. 5d shows a good conductivity of LCC@MnO_2 symmetric supercapacitor. Usually, in order to compare the high-frequency performance of a device, the cross-frequency at −45° of the impedance phase angle is used as a key indicator[9]. For LCC@MnO_2//MnO_2@LCC, the cross-frequency is found to be 212 Hz (Fig. 5e), indicating a good high-frequency property. Furthermore, the symmetrical capacitor could deliver a CA of 1.53 mF cm^{-2} at 120 Hz and a good cycle stability with over 92.10% capacitance retention after 100 000 cycles at 100 V s^{-1} (Fig. 5f). This performance of LCC@MnO_2 material makes it promise for high-frequency applications, where the supercapacitor is required to charge/discharge at 120 Hz.

To evaluate the mechanical flexibility of the LCC@MnO_2 symmetric supercapacitor, bending tests are performed (Fig. 6a) at different bending angles

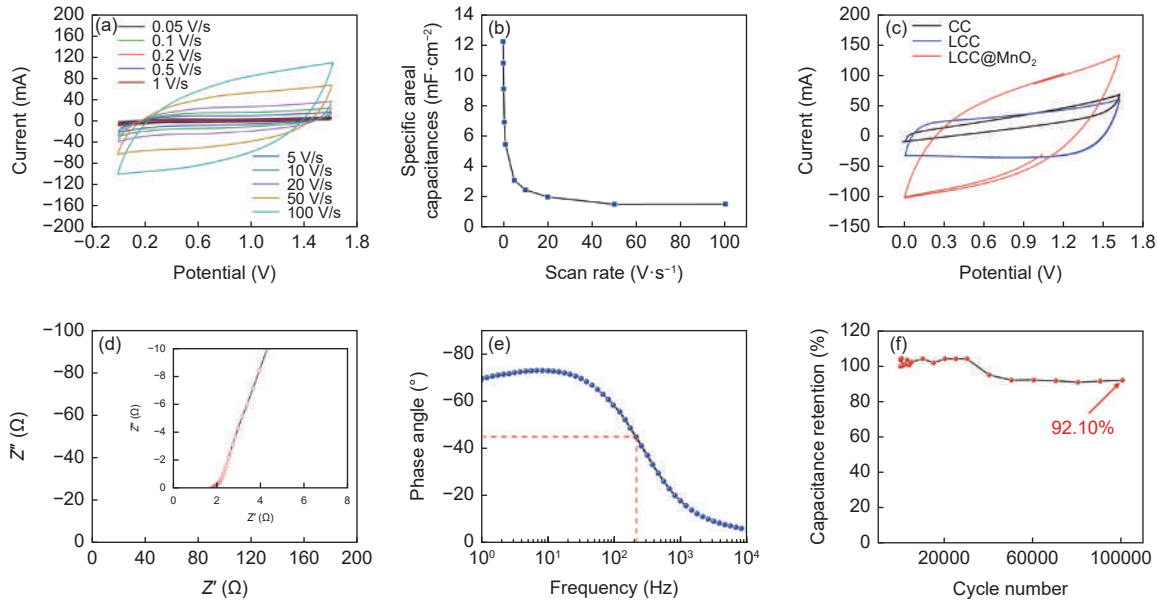

Fig. 5　(a) CV curves of the LCC@MnO_2 symmetric supercapacitor at different scan rates 0.05-100 V s^{-1}. (b) The specific areal capacitance of the LCC@MnO_2 symmetric supercapacitor at different scan rates. (c) CV curves of CC, LCC and LCC@MnO_2 symmetric supercapacitors at 100V s^{-1}. (d) EIS characterization for the LCC@MnO_2 symmetric supercapacitor from 100 kHz to 0.01 Hz and inset is an enlarged view at the high frequency range. (e) Plots of phase angle versus frequency of LCC@MnO_2 symmetric supercapacitor. (f) Cycling stability of the LCC@MnO_2 symmetric supercapacitor at 100 V s^{-1}.

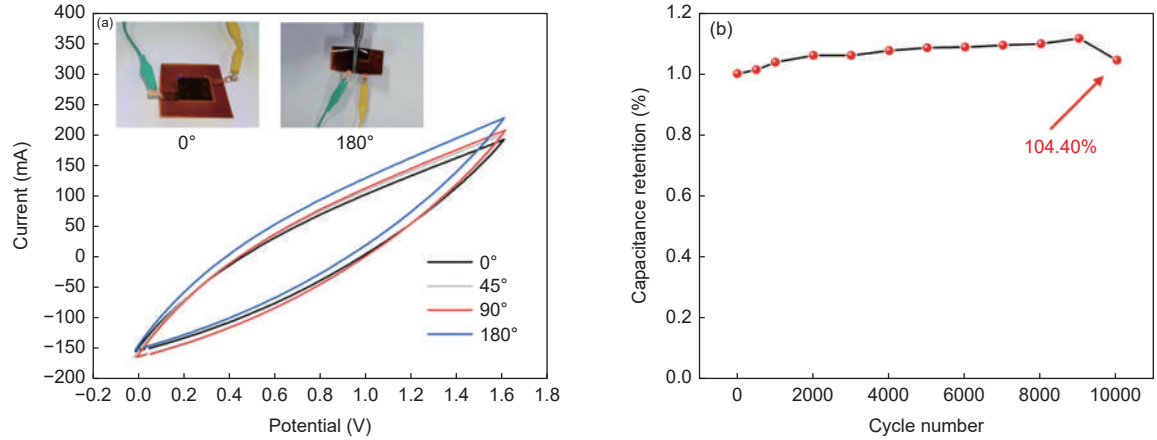

Fig. 6　(a) CV curves at 100V s^{-1} of the LCC@MnO_2 symmetric supercapacitor at different bending angles (0°, 45°, 90° or 180°). (b) Cycle stability of the LCC@MnO_2 symmetric supercapacitor at 100 V s^{-1}.

(0°, 45°, 90° or 180°) at 100 V s^{-1}. Consequently, the CV curves keep the constant shape, indicating that the favorable flexibility. CV testing at 100 V s^{-1} for 10 000 cycles is conducted to assess the electrochemical stability of the electrode (Fig. 6b). This flexible supercapacitor displays distinguished cycle stability, which maintains 104.40% capacitance retention after cycling for 10 000 times. In a nutshell, this symmetric supercapacitor based on LCC@MnO_2 exhibits excellent flexibility and electrochemical performance.

4 Conclusion

We have put forward a fast strategy through defocused laser ablation for supercapacitors used at high-frequency. Because of the synergistic effects of the CC and the MnO_2 nanosheets, the LCC@MnO_2 symmetric supercapacitor exhibits an excellent CA performance of 1.53 mF cm^{-2} at 120 Hz and excellent cycle stability (92.10% capacitance retention after 100 000 cycles at 100 V s^{-1}), which have reached the standards of commercial tantalum capacitors (1.5 mF cm^{-2} at 120 Hz). When encapsulated in the flexible device, the device shows an excellent flexibility (0°-180°) and stable cyclic stability (104.40% capacitance retention after 10 000 cycles at 100 V s^{-1}). In view of the high flexibility and excellent high-frequency specific area capacitance, this electrode based on LCC@MnO_2 is believed to have huge potential in the applications of flexible, lighter, and faster electronic devices.

Acknowledgements

The authors thank the National Natural Science Foundation of China (52061160482), the Tsinghua University Spring Breeze Fund, the Local Innovative and Research Teams Project of Guangdong Pearl River Talents Program (2017BT01N111), Guangdong Provincial Key Laboratory of Thermal Management Engineering & Materials (2020B1212060015), Shenzhen Technical Project (JSGG20191129110201725) and Shenzhen Geim Graphene Center for financial supports..

References

[1] Xu S X, Liu W, Hu B M, et al. Circuit-integratable high-frequency micro supercapacitors with filter/oscillator demonstrations[J]. Nano Energy, 2019, 58: 803-810.

[2] Lu P, Xue H, Liu W, et al. Chemically roughened, sputtered Au films with trace-loaded manganese oxide for both on-chip and off-chip high frequency supercapacitors[J]. Nanomaterials, 2021, 11(2): 257-264.

[3] Sun Z, Firdoz S, Yap E Y, et al. Hierarchically structured MnO_2 nanowires supported on hollow Ni dendrites for high-performance supercapacitors[J]. Nanoscale, 2013, 5(10): 4379-4387.

[4] Xu B, Yu L, Sun M, et al. One-pot hydrothermal synthesis of novel 3D starfish-like δ-MnO_2 nanosheets on carbon fiber paper for high-performance supercapacitors[J]. RSC Advances, 2017, 7(24): 14910-14916.

[5] Zhao G Y, Wang F C, Zhang Y Y, et al. High-performance hydrogen peroxide micro-sensors based on laser-induced fabrication of graphene@Ag electrodes[J]. Applied Surface Science, 2021, 565: 150565.

[6] Chyan Y, Ye R, Li Y, et al. Laser-induced graphene by multiple lasing: Toward electronics on cloth, paper, and food[J]. ACS Nano, 2018, 12(3): 2176-2183.

[7] Zhang J, Sun J B, Shifa T A, et al. Hierarchical MnO_2/activated carbon cloth electrode prepared by synchronized electrochemical activation and oxidation for flexible asymmetric supercapacitors[J]. Chemical Engineering Journal, 2019, 372: 1047-1055.

[8] Chen Z, Zheng L, Zhu T, et al. All-solid-state flexible asymmetric supercapacitors fabricated by the binder-free hydrophilic carbon cloth@MnO_2 and hydrophilic carbon cloth@polypyrrole electrodes[J]. Advanced Electronic Materials, 2019, 5(3): 1800721.

[9] Han Z J, Huang C, Meysami S S, et al. High-frequency supercapacitors based on doped carbon nanostructures[J]. Carbon, 2018, 126: 305-312.